RSC Advances

PAPER

View Article Online
View Journal | View Issue

Cite this: *RSC Adv.*, 2017, **7**, 33402

Structural, mechanical and electronic properties of Nb_2C: first-principles calculations†

Xiaojing Sha, Namin Xiao, Yongjun Guan and Xiaosu Yi*

Received 25th May 2017
Accepted 16th June 2017

DOI: 10.1039/c7ra05856j

rsc.li/rsc-advances

Nb–C compounds are potential candidates to achieve high hardness and refractory nature. We performed a crystal structure search for the Nb–C system using an *ab initio* evolutionary algorithm implemented in the USPEX code. By comparing the formation enthalpy, a *P–x* phase diagram was calculated, and an orthorhombic *Pnnm* structure of Nb_2C was predicted and denoted as Nb_2C-*I*, which was both mechanically and dynamically stable. In this *Pnnm* phase, there are four-sided rings continuously along the *c*-axis, which probably contributes to the relatively high incompressibility of Nb_2C-*I* along the crystallographic *c*-axis. Moreover, the hardness and Young's modulus were calculated to be 28.5 GPa and 448.9 GPa, respectively; hence, the Nb_2C-*I* is considered as a potential ultra-stiff and hard material.

1 Introduction

In the past few decades, superhard materials with excellent mechanical properties have drawn extensive attention from the researchers and have been well-studied in terms of both theoretical and experimental aspects.[1] Traditional superhard materials, such as diamond,[2,3] γ-B,[4] *c*-BN,[5] and *c*-BC_2N,[6,7] are mainly composed of light elements. Diamond, the earliest discovered and hardest (70–150 GPa) superhard material, shows promising mechanical properties and is hence among the most widely used superhard materials. However, diamond shows its own practical defects. At a temperature greater than 800 °C, diamond tends to oxidize. Moreover, when the diamond tool is used in the grinding or cutting of ferrous materials, the tool easily reacts with iron-based materials. The *c*-BN, another typical superhard material, is difficult to synthesise, which limits its practical application. Therefore, development of novel superhard multifunctional materials is an urgent requirement.

During the past decade, scientists were focused on the design of new materials in transition-metal (TM) light-element (LE) systems. One of the advantages of transition metals is their large bulk modulus. For example, the bulk modulus of Os is about 395–462 GPa,[8] which is close to that of diamond (446 GPa). However, the hardness of metal is always low, which is normally one-thirtieth that of diamond. This is mainly due to the huge difference of chemical bonds in the compound structures. Classical superhard materials usually hold three-dimensional networks composed of covalent bonds with sp^3 hybridization, which is the basis of superhard properties. Therefore, the type of TM-LE bonding is the key factor for improving the hardness. Due to the behavior of high valence electron density and large interatomic distance, the transition metal can be intercalated with light elements, which may lead to the formation of covalent bonding between light elements and transition metals. Thus, the relatively high directional covalent bonds and valence electron density are considered to favor the formation of new superhard materials. It is believed that the carbides of the group-IV, -V, and -VI transition metals show an unusual combination of physical and chemical properties.[9–14] The transition-metal carbide (TMC) compounds combine the physical properties of three different kinds of materials: transition metals, covalent solids and ionic crystals,[15] making TMC a family of industrially relevant compounds with outstanding physical properties.

The niobium carbides are an emblematical TMC system, which exhibits meaningful physicochemical properties.[10,16] Moreover, niobium carbides are significant candidates for improving the mechanical properties of niobium alloys.[10,16–19] Niobium and carbide could form weak metallic or semiconductors compounds with different compositions and space symmetries. In the Nb–C binary phase diagram, niobium carbides have four experimentally known compositions: NbC, Nb_6C_5, Nb_4C_3, and Nb_2C.[20–22] Stoichiometric NbC is in the rocksalt structure,[23] in which Nb atoms form the cubic lattices, and C atoms occupy the octahedral interstitial positions. Nb_4C_3 was reported to adopt a $R\bar{3}m$ space group, and Nb_6C_5 is in the $P3_1$ space group.[24,25] Among all the niobium carbides, Nb_2C is the least understood carbide;[26] it exists in three polymorphic forms: γ-Nb_2C, β-Nb_2C, and α-Nb_2C,[27–31] as reported in previous studies. The γ- and β-Nb_2C are hexagonal phases. The γ-Nb_2C is in L'3-type structure at temperatures above 2770 K. The β-Nb_2C has ζ-Fe_2N structure at relatively low temperatures. The α-Nb_2C is an orthorhombic low temperature phase. As Hugosson reported,[20]

Materials Genome Center, Beijing Institute of Aeronautical Materials, Beijing, P. R. China. E-mail: yi_xiaosu@sina.cn

† Electronic supplementary information (ESI) available. See DOI: 10.1039/c7ra05856j

some controversy exists in the determination of the structure of the orthorhombic phase. In his study, both structures showed energies of formation higher than those of the hexagonal phase. However, other studies showed that the formation energy of α-Nb_2C was the lowest, which indicated that the formation of α-Nb_2C was feasible.[26,32] To date, controversy still remains regarding the orthorhombic phase structure of Nb_2C.

In this article, we performed a crystal structure search for the Nb–C system using an *ab initio* evolutionary algorithm implemented in the USPEX code. Full *P*–*x* phase diagrams of the Nb–C system at 0 K were calculated. We report a new phase for Nb_2C at high pressures. The predicted new phase of Nb_2C belongs to the orthorhombic *Pnnm* space group. Moreover, this phase is dynamically and mechanically stable at ambient and high pressures. Through a detailed electronic structure analysis, we found that niobium and carbon formed strong bonds with sp^3 hybridization style, which further knitted into three-dimensional networks. Collectively, we proved that Nb_2C can be a potential candidate for an ultra-stiff and hard material.

2 Methods

To search the stable and low-enthalpy structures of the Nb–C system, the evolutionary algorithm USPEX[33–35] coupled with an *ab initio* evolutionary algorithm (EA) was employed. The calculation was designed to find the most stable structure for the given stoichiometries under given external conditions as implemented in the USPEX code. In this study, evolutionary crystal structure prediction calculations were performed at 0, 10, 30, and 50 GPa for the Nb_xC_y system ($x = 1$–8, $y = 1$–8) at zero temperature. We performed *ab initio* calculations with the local density approximation (LDA), as implemented in the Vienna *ab initio* simulation package (VASP) code,[36,37] which is based on density functional theory. The electron–ion interaction was described *via* the projector augmented wave (PAW) scheme.[38] The orbitals 2s and 2p for C and 4p, 4d, and 5s for Nb were treated as valence states. During structural relaxation, a tested energy cutoff of 600 eV was used for the plane wave basis sets, and Monkhorst–Pack[39] *k*-point meshes with a resolution of 0.03 $Å^{-1}$ in the reciprocal space were used for all structures to minimize error from the *k*-point meshes. The atomic positions, lattice parameters, and cell volume were fully relaxed until the force on each atom was less than 1 meV $Å^{-1}$. Phonons were calculated using the supercell method implemented in the PHONOPY package.[40,41] The strain–stress method was used to calculate the elastic constants. The shear modulus, bulk modulus, Young's modulus, and Pugh's indicator were derived from the Voigt–Reuss–Hill approximation.[42–44] The structure diagram of Nb_2C was drawn using VESTA.[45]

3 Results and discussion

In this study, we uncovered a stable structure of Nb_2C, denoted as Nb_2C-*I*. At first, we calculated the formation enthalpy of Nb_xC_{1-x} using a fractional representation of Nb_xC_{1-x} with respect to its decomposition into Nb and C as

$$\Delta H(Nb_xC_{1-x}) = H(Nb_xC_{1-x}) - [x \times H(Nb) + (1 - x) \times H(C)]$$

where x is the concentration of Nb. The formation enthalpies from 0 to 50 GPa were evaluated as the difference in the enthalpy of the predicted Nb–C system with respect to Nb metal and C in their most stable forms (bcc phase for Nb and graphite for C), as depicted in Fig. 1. The formation enthalpy of NbC

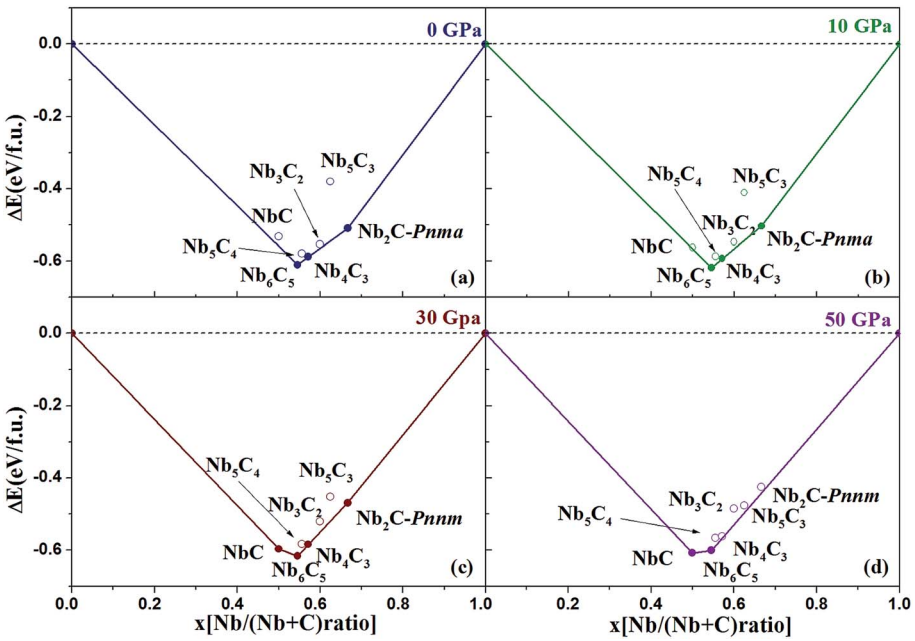

Fig. 1 Convex hull diagram for the Nb–C compounds. The formation enthalpies (Δ*H*, with respect to Nb and C of their most stable phases) of Nb_xC_{1-x}. The abscissa *x* is the fraction of Nb in the structures. Circles on the solid lines represent stable ground-state compounds.

(*Fm3m*) in our calculation is −0.531 eV, similar to the previous results[20] (−43 mRy = −0.585 eV). Structures lying on the convex hull are either thermodynamically stable or metastable and can be synthesized in principle. According to Fig. 1(a), at 0 GPa, the Nb_2C-*Pnma* and Nb_6C_5 phases are thermodynamically stable, and Nb_4C_3 is also located on the convex hull, which is similar to the previous results.[32] With an increase in the pressure, the stoichiometric NbC phase becomes thermodynamically stable, and Nb_2C-*Pnnm* is more stable than Nb_2C-*Pnma* at 30 GPa. We calculated the formation enthalpies of three candidates of Nb_2C. As Fig. 2 shows, the enthalpy curves of Nb_2C structures are presented. It can be clearly seen that the Nb_2C-*Pnma* is the most stable structure at 0 GPa, which is consistent with the Wu's studies.[22] When the pressure is greater than 15.8 GPa, the formation enthalpies of the proposed Nb_2C-*I* are lowest negative values, which indicates that Nb_2C-*I* is thermodynamically stable under pressure. From Fig. 1(d), it can be observed that at 50 GPa, the stable phases are only NbC and Nb_6C_5. We calculated the detailed enthalpy differences as a function of pressure. As shown in the ESI Fig. S1(a),† the enthalpy difference of NbC is calculated against decomposition into Nb_6C_5 and C; thus, we concluded that the NbC phase becomes stable at 12.3 GPa. The enthalpy differences of Nb_4C_3 and Nb_2C-*Pnnm* are calculated against decomposition into the constituent carbides. As shown in Fig. S1(b) and (c),† the structures of Nb_4C_3 and Nb_2C-*Pnnm* become completely unstable at 39.7 GPa and 40.5 GPa, respectively. With these detailed calculations shown in Fig. S1,† a pressure–constituent (*P*–*x*) phase diagram of niobium carbide was constructed, which is plotted in Fig. 3. With the increase in C concentration, the Nb–C system first undergoes an orthorhombic to monoclinic transition and then transforms back to the cubic phase. Moreover, some phases of niobium carbides appear and decompose with the increase of pressure. However, the structure with high carbon concentration is not stable, even if the pressure is increased to 50 GPa.

The *Pnnm* structure, as we predicted, contains two Nb_2C in a unit cell at 20 GPa (a = 5.415 Å, b = 4.837 Å, and c = 3.019 Å), in which two inequivalent atoms Nb and C occupy the Wyckoff

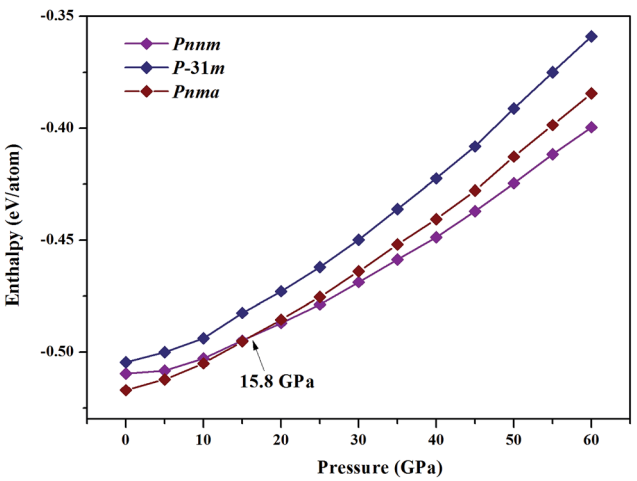

Fig. 2 Enthalpy–pressure diagrams. Calculated enthalpies as the function of pressure.

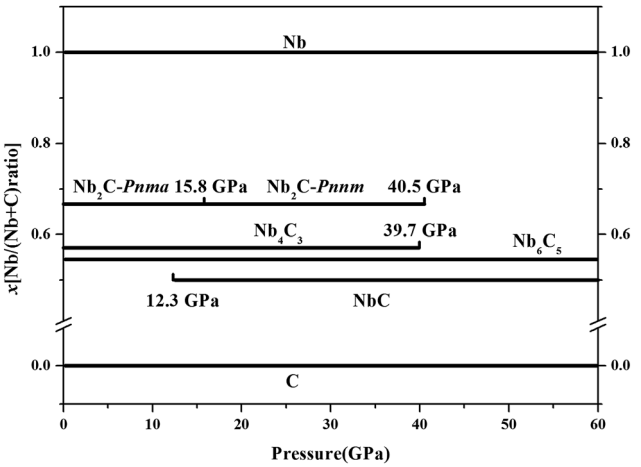

Fig. 3 Pressure–composition phase diagrams.

8h (0.3462, 0.7632, 0.5000) and 2b (0.5, 0.5, 0.0) sites, as summarized in Table 1 and shown in Fig. 4. Fig. 4(b) along the *y*-axis and Fig. 4(c) along the *z*-axis reveal a fundamental structure in the *Pnnm* phase. Fig. 4(d) shows the structure of *Pnma* phase along the *y*-axis. When we compared Fig. 4(b) with (d), it was observed that the carbon atoms in Nb_2C-*Pnnm* could help to achieve better formation of the three-dimensional space grid structure, which avoided the appearance of the interaction between metal atoms.

It is well-known that the phonon dispersion curves give information about the global structural stability of the materials. As shown in Fig. 5, we analyzed the phonon dispersion curves to test the lattice dynamical stability of Nb_2C-*I* at 0 and 20 GPa. The calculated phonon curves of Nb_2C have no soft mode in the Brillouin zone, indicating that Nb_2C is dynamically stable. For the purpose of understanding the mechanical properties, the elastic constants are deemed essential. The elastic constants C_{ij} of the *Pnnm* phases are listed in Table 2. For the proposed Nb_2C-*Pnnm*, all C_{ij} satisfy Born–Huang criteria,[46] which means that the proposed Nb_2C-*Pnnm* is mechanically stable. We determined that the Nb_2C-*Pnnm* could be synthesized under high pressure and preserved under ambient pressure. From Table 2, it can be found that the calculated C_{33} value is bigger than the values of C_{11} and C_{22}, indicating that there is relatively high incompressibility along the *c*-axis. The relative high incompressibility of the proposed Nb_2C along the *c*-axis is perhaps contributed by the existence of four-sided rings, which are continuously along the crystallographic *c*-axis. In contrast, four-sided rings and eight-sided rings exist alternately along the *b*-axis or *c*-axis. Therefore, there is certain disparity between C_{33} and C_{11} (or C_{22}).

It is well-known that superhard materials should have high bulk modulus and high shear modulus to resist the volume change and shape change. At 0 and 20 GPa, the bulk modulus of Nb_2C-*Pnnm* is 244 and 310 GPa, respectively, which are larger than the values of Nb_2C-*Pnma* (236 and 304 GPa, respectively). Because the value of the bulk modulus is large, Nb_2C can be grouped into incompressible materials. As reported in Table 2,

Table 1 The optimized equilibrium lattice constants *a*, *b*, and *c* (Å), and atomic coordinates for Nb_2C-*I* at 20 GPa

	Structure	Parameters (Å)	Atom	*x*	*y*	*z*
Nb_2C	*Pnnm* (orthorhombic)	$a = 5.415$, $b = 4.837$, $c = 3.019$	Nb(8h)	0.3462	0.7632	0.5000
			C(2b)	0.5000	0.5000	0.0000

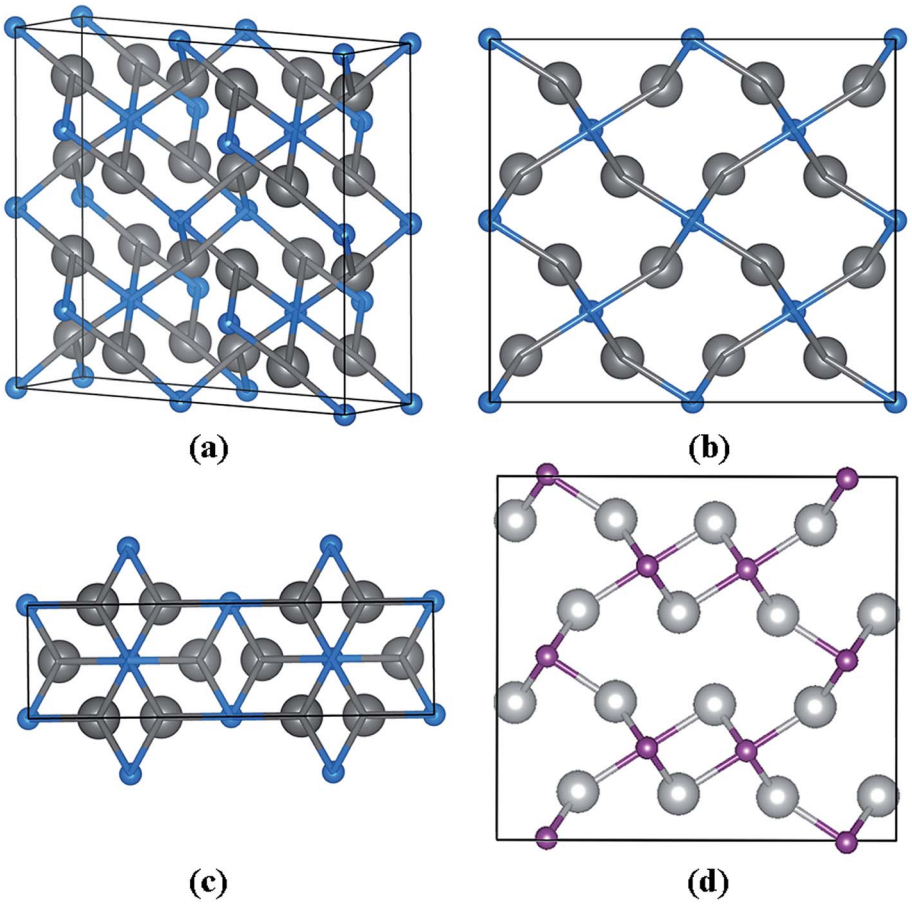

Fig. 4 Crystal structures of the predicted Nb_2C-*Pnnm*. (a) The structure of Nb_2C-*Pnnm*. (b) The structure along the *y*-axis. (c) Along the *z*-axis. The large gray and small blue spheres represent the Nb and C atoms, respectively. (d) The structure of Nb_2C-*Pnma* along the *y*-axis.

the Poisson's ratio ν of Nb_2C-*Pnnm* is about 0.19. Usually, strong directionality degree of covalent bonding is considered in the materials when the ν value is near 0.2, indicating that the directionality degree of covalent bonding of Nb_2C-*Pnnm* is strong. The Pugh's indicator G/B of Nb_2C is 0.77, which is a relatively large value. According to the Pugh's modulus ratio defined by Cheng *et al.*,[47] the Nb_2C-*I* phase is a brittle and hard material with a huge capability to resist elastic plastic deformation. To gain a more comprehensive and profound understanding of the mechanical property, we calculated the Vickers hardness of Nb_2C-*I*. The Vickers hardness H_V, estimated by the empirical model, was obtained by the following formula:

$$H_V = (k^2G)^{0.585} - 3 \ (k = G/B)$$

The calculated hardness of Nb_2C-*I* is 28.5 GPa, which almost matches that of the hard material WC (21.5–33.4 GPa).[47,48] Our results suggested that the proposed Nb_2C-*I* could be a potential candidate for ultra-stiff and hard materials.

The electronic structure is crucial to understand the origin of physical properties of these carbides. The total and site projected electronic densities of states (PDOS) of Nb_2C-*I* are shown in Fig. 6(a). As the graphic shows, Nb_2C is a metal as the d electronics of Nb are mainly attributed to the density near the Fermi energy in our calculation model. To determine the hybridization between C and Nb, projected electronic densities of states of the nearest Nb and C are calculated, as shown in Fig. 6(b). There is an obvious hybridization between C 2p and Nb 4d states, which is a common feature of typical TMC superhard materials. To obtain more information about the bonding character, the electronic localization function (ELF) of Nb_2C-*I* was calculated, as shown in Fig. 7. The electron localization function between Nb atoms and C atoms has a slight increase as compared to that in the background, which

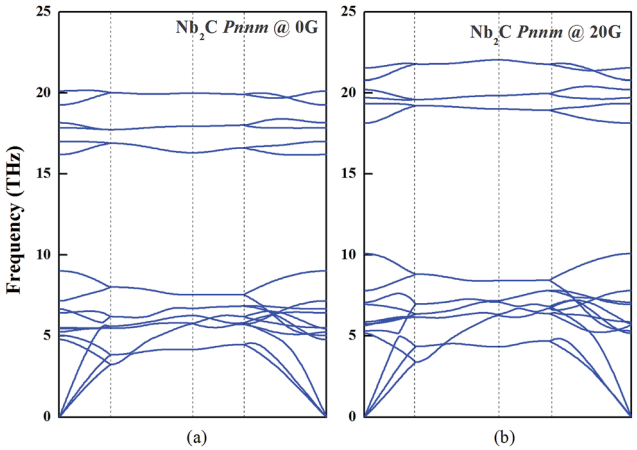

Fig. 5 Dynamic stability of Nb_2C-*I*. The phonon dispersion curves of Nb_2C-*I* along the high symmetry directions of the Brillouin zone at 0 and 20 GPa.

Table 2 Elastic constants C_{ij}, Poisson's ratio ν, bulk modulus B (GPa), shear modulus G (GPa), Pugh's indicator G/B, Young's modulus E (GPa), and Vickers hardness H_V of Nb_2C-*Pnma* and Nb_2C-*Pnnm* at 0 GPa

	C_{11}	C_{22}	C_{33}	C_{44}	C_{55}	C_{66}	C_{12}	C_{13}	C_{23}
Pnma	390	405	390	76	119	122	157	129	136
Pnnm	383	389	415	101	102	137	156	153	127

	ν	B	G	G/B	E	H_V
Pnma	0.19	236.1	178.1	0.75	426.9	26.8
Pnnm	0.19	244.5	188.0	0.77	448.9	28.5

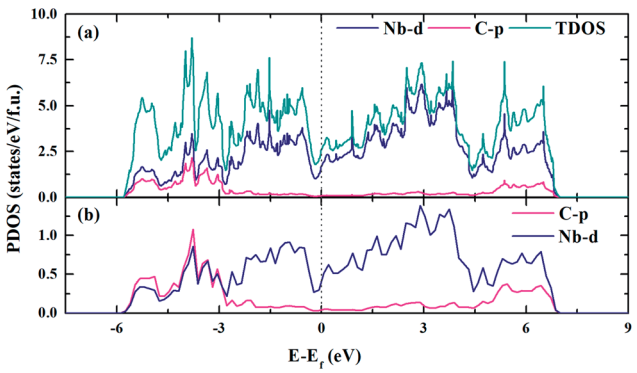

Fig. 6 Electronic density of states of Nb_2C-*I*. The DOS (a) and PDOS (b) of Nb_2C-*I*. The vertical black dashed line denotes the Fermi level.

indicates that mixed bonds between the two atoms are present in this area, in which the ionic bonds are dominant. As Becke defined,[49] the electrons can move freely in the areas of ELF = 0.5. In Fig. 7(a), the green region is almost connected. However, there are disconnected equivalent spheres in Fig. 7(b). In total, the equivalent sphere of ELF = 0.5 is

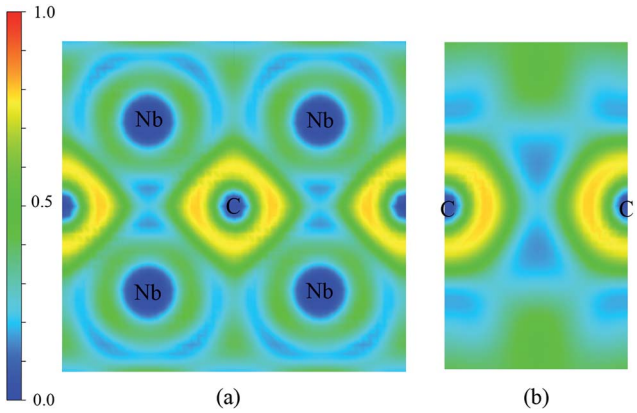

Fig. 7 Contours of the electronic localization functions (ELF). Electron localization function isosurface maps for (a) Miller indices: (1.67 1 0) and (b) Miller indices: (1 0 0).

partially connected in the whole crystal, which may enhance the weak metallicity properties.

4 Summary

In summary, we researched the full-scale zero-temperature Nb–C phase diagram using an *ab initio* evolutionary algorithm implemented in the USPEX code. The *P–x* phase diagrams of the Nb–C system are constructed. A new structure of Nb_2C has been uncovered and denoted as Nb_2C-*I*. The Nb_2C-*I* belongs to the orthorhombic system with the space group *Pnnm*. Phase stability, mechanical properties, and electronic properties of Nb_2C-*I* were investigated. The Vickers hardness and Young's modulus of Nb_2C-*I* have been calculated to be 28.5 GPa and 448.9 GPa, respectively, which prove that Nb_2C-*I* can be considered as low compressible materials. We considered that the formation of continuous four-sided rings along the *c*-axis might cause high incompressibility of Nb_2C-*I* in the *c*-axis direction. A deep analysis of the electronic density of states and chemical bonding indicates that an ionic bond is dominant in the Nb_2C crystals.

Acknowledgements

This work was supported by the National Key Research and Development Program of China (No. 2016YFB0700505, 2016YFB0701401). Parts of the results described in this paper are obtained on the Era of Computer Network Information Center of Chinese Academy of Sciences.

References

1 V. V. Brazhkin, A. G. Lyapin and R. J. Hemley, *Philos. Mag. A*, 2002, **82**, 231–253.
2 N. Mounet and N. Marzari, *Phys. Rev. B: Condens. Matter Mater. Phys.*, 2005, **71**, 205214.
3 V. Brazhkin, N. Dubrovinskaia, A. Nicol, N. Novikov, *et al.*, *Nat. Mater.*, 2004, **3**, 576–577.

4 J. Qin, N. Nishiyama, H. Ohfuji, *et al.*, *Scr. Mater.*, 2012, **67**(3), 257–260.
5 J. C. Zheng, *Phys. Rev. B: Condens. Matter Mater. Phys.*, 2005, **72**, 052105.
6 V. L. Solozhenko, D. Andrault, T. G. Fique, *et al.*, *Appl. Phys. Lett.*, 2001, **78**(10), 1385–1387.
7 Z. Pan, H. Sun and C. Chen, *Phys. Rev. Lett.*, 2007, **98**(13), 135505.
8 F. Occelli, D. L. Farber, J. Badro, *et al.*, *Phys. Rev. Lett.*, 2004, **93**(9), 095502.
9 W. Weber, *Phys. Rev. B: Solid State*, 1973, **8**, 11.
10 L. E. Toth, *Transition Metal Carbides and Nitrides*, Academic Press, New York, 1971.
11 S. T. Oyama, *Catal. Today*, 1992, **15**, 179.
12 Z. Zhao, K. Bao, F. Tian, D. Duan, B. Liu and T. Cui, *Phys. Rev. B: Condens. Matter Mater. Phys.*, 2016, **93**, 214104.
13 Y. Liang, J. Yang, X. Yuan, W. Qiu, Z. Zhong, J. Yang and W. Zhang, *Sci. Rep.*, 2014, **4**, 5063.
14 S. Wang, D. Antonio, X. Yu, J. Zhang, A. L. Cornelius, D. He and Y. Zhao, *Sci. Rep.*, 2015, **5**, 13733.
15 H. Hwu and J. G. Chen, *Chem. Rev.*, 2005, **105**, 185–212.
16 E. K. Storms, *The Refractory Carbides*, Academic Press, New York-London, 1967.
17 E. J. Delgrosso, C. E. Carlson and J. J. Kaminsky, *J. Less-Common Met.*, 1967, **12**, 173.
18 F. C. Campbell, *Elements of Metallurgy and Engineering Alloys*, ASM International, Ohio, 2008.
19 V. Javaheri, F. Shahri, M. Mohammadnezhad, M. Tamizifar and M. Naseri, *J. Mater. Eng. Perform.*, 2014, **23**, 3558–3566.
20 H. W. Hugosson, O. Eriksson, U. Janssion and B. Johansson, *Phys. Rev. B: Condens. Matter Mater. Phys.*, 2001, **63**, 134108.
21 H. W. Hugosson, U. Jansson, B. Johansson and O. Eriksson, *Chem. Phys. Lett.*, 2001, **333**, 444–450.
22 L. Wu, Y. Wang, Z. Yan, J. Zhang, F. Xiao and B. Liao, *J. Alloys Compd.*, 2013, **561**, 220–227.
23 H. M. Ledbetter, S. Chevacharoenkul and R. F. Davis, *J. Appl. Phys.*, 1986, **60**, 1614–1617.
24 A. N. Christensen, *Acta Chem. Scand., Ser. A*, 1985, **39**, 803–804.
25 K. Yvon and E. Parthé, *Acta Crystallogr., Sect. B: Struct. Sci.*, 1970, **26**, 149–153.
26 B. Vishwanadh, T. S. R. C. Murthy, A. Arya, R. Tewari and G. K. Dey, *J. Alloys Compd.*, 2016, **671**, 424–434.
27 J. F. Smith, O. N. Carlson and D. R. R. Avillez, *J. Nucl. Mater.*, 1987, **148**, 1–16.
28 E. Parthe and K. Yvon, *Acta Crystallogr., Sect. B: Struct. Sci.*, 1970, **26**, 153–163.
29 E. Rudy and C. E. Brukl, *J. Am. Ceram. Soc.*, 1967, **50**, 265–268.
30 N. Terao, *Jpn. J. Appl. Phys.*, 1964, **104**, 104–111.
31 B. Lonnberg and T. Lundstrom, *J. Less-Common Met.*, 1985, **113**, 261–268.
32 X. Yu, C. R. Weinberger and G. B. Thompson, *Comput. Mater. Sci.*, 2016, **112**, 318–326.
33 A. R. Oganov and C. W. Glass, *J. Chem. Phys.*, 2006, **124**, 244704.
34 A. R. Oganov, C. W. Glass and S. Ono, *Earth Planet. Sci. Lett.*, 2006, **241**, 95–103.
35 C. W. Glass, A. R. Oganov and N. Hansen, *Comput. Phys. Commun.*, 2006, **175**, 713–720.
36 G. Kresse and D. Joubert, *Phys. Rev. B: Condens. Matter Mater. Phys.*, 1999, **59**, 1758–1775.
37 G. Kresse and J. Furthmuller, *Phys. Rev. B: Condens. Matter Mater. Phys.*, 1996, **54**, 11169–11186.
38 P. E. Bloch, *Phys. Rev. B: Condens. Matter Mater. Phys.*, 1994, **50**, 17953–17979.
39 H. J. Monkhorst and J. D. Pack, *Phys. Rev. B: Solid State*, 1976, **13**, 5188–5192.
40 A. Togo, F. Oba and I. Tanaka, *Phys. Rev. B: Condens. Matter Mater. Phys.*, 2008, **78**, 134106.
41 A. Togo, *Phonopy*, https://atztogo.github.io/phonopy/.
42 R. Hill, *Proc. Phys. Soc., London, Sect. A*, 1952, **65**, 349–354.
43 *Lehrbuch der kristallphysik*, ed. W. Voigt, Teubner-Leipzig, New York, Macmillan, 1928, p. 739.
44 A. Reuss, *Z. Angew. Math. Phys.*, 1929, **9**, 49–58.
45 K. Momma and F. Izumi, *J. Appl. Crystallogr.*, 2011, **44**, 1272–1276.
46 Z. Wu, E. Zhao, H. Xiang, X. Hao, X. Liu and J. Meng, *Phys. Rev. B: Condens. Matter Mater. Phys.*, 2007, **76**, 054115.
47 X. Cheng, H. Niu, D. Li and Y. Li, *Intermetallics*, 2011, **19**, 1275–1281.
48 A. Simunek and J. Vackar, *Phys. Rev. Lett.*, 2006, **96**, 085501.
49 A. D. Becke and K. E. Edgecombe, *J. Chem. Phys.*, 1990, **92**, 5397.